Dear Reviewer 2:

We thank you for the critical feedback. Based on the comments we received, careful modifications have been made to our manuscript. All the changes were marked in red text.

We hope our revised manuscript will meet the standard of ***Electronics***. Below you will find point-by-point responses to the comments.

Manuscript ID: electronics-1932562

Title: Compact 8×8 MIMO Antenna Design for 5G Terminals

Response to the Comments of Reviewer 2

We appreciate Reviewer 2 for his or her comments and suggestions.

According to the Answers of Reviewer 2, we revised our manuscript carefully. Following is a summary of our responses to Reviewer 2.

Comments to the Author

Comments for Transmittal to Author

The topic “Compact 8×8 MIMO Antenna Design for 5G Terminals” presented in the paper using T-shaped monopole and dipole antennas for 5G terminals satisfies the MIMO parameters. But the following comments must be reported.

Response:

Thank the reviewers for their valuable comments, and we will answer each comment one by one.

Answer 1:

In figure 1, the geometry of the proposed MIMO antenna array, the yellow dots (circles) are not highlighted.

Response:

According to your comment, the figure is revised.

Answer 2:

Are there all four antennas T-shaped in each pair?

Response:

Each pair consists of two T-shaped antennas and two edge-coupled-fed dipole antennas. In Section 2, we mentioned that “each antenna pair consists of four antenna elements, which are two symmetrical T-shaped monopole-mode antenna elements and two symmetrical edge-coupled-fed dipole-mode antenna elements printed on the inner and outer sides of the side plates, respectively.”

Answer 3:

The axis labels are not same in the figures 3, 6, 9, and 11. There should be curve markers in figures 3, 6, 9, 11, 12, and 13.

Response:

According to your comment, the axis labels in figures are revised and the curve markers are added in figures.

Answer 4:

can the author provide the antenna gain measurement setup, such as an Anechoic chamber, etc.?

Response:

The prototype is measured with a vector network analyzer Agilent E8363B and a microwave chamber. According to your comment, we make the following revise in the manuscript as:

"…as shown in Figure 10. The prototype is measured with a vector network analyzer Agilent E8363B and a microwave chamber. Figure 11 presents…"

Answer 5:

It is suggested to discuss MIMO performance parameters such as diversity gain, etc.

Response:

The diversity gain result is added in the manuscript in Section 3 as:

"DG is an important parameter to measure good diversity characteristics and MIMO system performance. According to [30], DG can be calculated from Formula (2), and the ideal value of DG should be 10 dB.

$$DG = \sqrt{1-|\rho_e|^2} \quad (2)$$

"

"It can be seen from Figure 12 that diversity gain values are all around 10 dB, meeting the MIMO diversity criterion."

Answer 6:

Please correct the dimensions in the comparison table for reference [27].

Response:

According to your comment, we make the following revise in the manuscript in Table I:

Ref.	**Antenna Size(mm^2)**	**Integration**	**Isolation**	**Bandwidth**	**ECC**
[24]	20×7	Two-element integration	>17dB	3.4~3.6 GHz	<0.1
[25]	12×17	Two-element integration	>20dB	3.4~3.6 GHz	<0.06
[26]	25×7	Two-element	>20dB	3.4~3.6	<0.13

		integration		GHz	
[27]	60×5	Four-element integration	>10dB	3.3~7.2 GHz	<0.2
[28]	38.2×3.2	Four-element integration	>11.8dB	3.4~3.6 GHz	/
This work	**28.6×7**	**Four-element integration**	>10dB	3.4~3.6 GHz	<0.35

We have further revised and edited the text of the manuscript. We tried our best to improve the manuscript and made some changes. We hope that all the corrections will meet standard of ***Electronics***.

Yours sincerely,

Haifu Zhang, Li-Xin Guo, Pengfei Wang, and Hao Lu

electronics

MDPI

Type of the Paper (Article)

Compact 8×8 MIMO Antenna Design for 5G Terminals

Haifu Zhang[1,2], Li-Xin Guo[1,*], Pengfei Wang[2], and Hao Lu[1]

[1] Xidian University, Xi'an, 710071, China; zhflpp@163.com; lxguo@xidian.edu.cn; itluhao@163.com
[2] 54th Research Institute of CETC, Shijiazhuang Hebei 050081, China; wangpfhyy@163.com
* Correspondence: lxguo@xidian.edu.cn

Abstract: In this paper, a compact 8×8 MIMO antenna design for 5G terminals is proposed. The 8×8 MIMO antenna consists of two quad-element antenna pairs, each of which includes two symmetrical T-shaped monopole mode elements and two symmetrical edge-coupled fed dipole mode elements. The size of the quad-element antenna is 38×7×0.8 mm^3. T-shaped monopoles are decoupled by parasitic elements, and dipoles are decoupled by grounding strips. Meanwhile, both T-shaped monopoles and dipoles are also decoupled by orthogonal mode. The results show that the operating frequency band of each antenna element meets the requirements of 3.4-3.6GHz, the reflection coefficient is less than -6dB, and the isolation between any antenna elements is more than 10dB. The antenna radiation efficiency is over 50% in the entire operating frequency band for the 8×8 MIMO system.

Keywords: multi-input multi-output (MIMO); polarization diversity; compact antenna; parasitic element

1. Introduction

With the continuous improvement of mobile communication quality requirements, the fifth generation (5G) mobile communication technology provides a promising solution for high communication rate, low latency, large connection density and high communication capacity. In order to meet the goals of 5G mobile communication and effectively improve the channel capacity of the communication system in a rich scattering environment, MIMO technology has become a key technology in the new generation of wireless communication systems [1]. Generally, the MIMO systems enlarge the channel capacity by its multiple independently placed elements which named as spatial diversity. However, due to the narrow space of the terminals, spatial diversity cannot reach its true potential. Thus, other diversity techniques as polarization diversity, radiation pattern diversity are applied in MIMO systems. Both the transmitter and the receiver of a MIMO system need to place multiple antennas, and the coupling between the antennas will reduce the performance of the MIMO system [2]. Therefore, the decoupling design of the MIMO antenna has become an important part of the wireless communication system. With the increase in the number of antennas on smart devices and the miniaturization of terminal equipment, the space left for antenna placement is limited. How to reduce mutual coupling between antennas and achieve high isolation in a compact space is a difficult problem.

Traditional decoupling methods such as neutralization line [3-5], parasitic element [6-8], EBG electromagnetic band gap [9-11], DGS defect ground structure [12-15] and decoupling network technology [16-18] all need to add additional decoupling structures in the middle of the antenna, which increases the complexity of the design. The occupied area of the antenna is large, and it cannot well meet the compact requirements of the future 5G terminal antenna.

Most of the initial polarization diversity technologies [19-22] use the same antenna elements placed orthogonally to achieve decoupling, which undoubtedly increases the occupied area of the antenna. Therefore, researchers use different antenna elements to achieve polarization diversity through their orthogonal current modes, which enhances

Citation: Lastname, F.; Lastname, F.; Lastname, F. Title. *Electronics* **2022**, *11*, x. https://doi.org/10.3390/xxxxx

Academic Editor: Firstname Lastname

Received: date
Accepted: date
Published: date

Publisher's Note: MDPI stays neutral with regard to jurisdictional claims in published maps and institutional affiliations.

Copyright: © 2022 by the authors. Submitted for possible open access publication under the terms and conditions of the Creative Commons Attribution (CC BY) license (https://creativecommons.org/licenses/by/4.0/).

the isolation and improves the compactness of the antenna.

In this paper, the polarization diversity is combined with the parasitic element to reduce the isolation of the designed compact MIMO antenna. The antenna integrates two T-shaped monopole elements and two edge-coupled dipole mode elements on an area of 28.6×7 mm², which greatly improves the integration degree of the antenna design. The orthogonal current modes of two types of elements enhance the isolation. Besides, parasitic elements and grounding strips are used to weaken coupling between elements of the same type. The operating frequency band of each element meets 3.4-3.6GHz with the S_{11} less than -6dB. The isolation between any elements is above 10dB. The simulation has been performed with the help of Ansys HFSS [23]. This article is organized as follows. This article is organized as follows. Section 2 describes the antenna configuration and decoupling principles. Section 3 presents the experimental results and discussions. Finally, Section 4 is the conclusion of this paper.

2. Antenna Configuration and Decoupling Principle

Figure 1 shows the overall structure and detailed dimensions of the eight-element highly integrated antenna. As shown in the Figure 1, the antenna consists of two 4-element highly integrated antenna pairs, and each antenna pair consists of four antenna elements, which are two symmetrical T-shaped monopole-mode antenna elements and two symmetrical edge-coupled-fed dipole-mode antenna elements printed on the inner and outer sides of the side plates, respectively. The material of the substrate is FR4. The size of the substrate is 150×75×0.8 mm³ and the area of the ground is 150×73 mm². Metal ground is printed on the back of the main board, and the width of the clearance area is only 1mm. Two small FR4 dielectric side plate with a size of 38×7×0.8 mm³ are installed along the left and right sides of the ground plane.

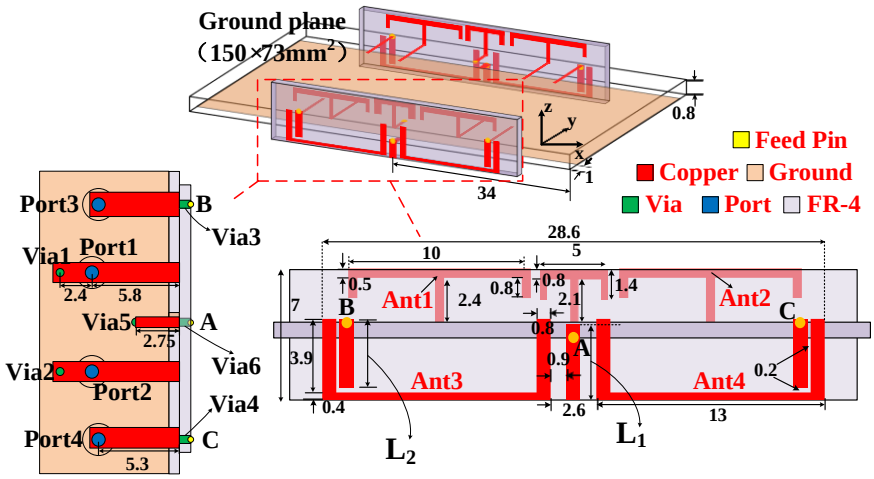


Figure 1. Geometry of the proposed MIMO antenna array.

The overall occupied area of the compact antenna pair is 28.6×7 mm². Ant1 and Ant2 are two symmetrical T-shaped monopole mode antenna elements, and each antenna element occupies an area of 10×2.9 mm². A 50 Ω microstrip line is used to directly feed Ant 1 and Ant 2 to form a monopole current mode. Microstrip lines with a length of 2.4 mm are extended at port 1 and port 2, respectively. They are connected to the metal ground through the metallized Via1 and Via2 to adjust the operating band of the monopole mode antenna element while improving the impedance matching. A T-type parasitic element is introduced between Ant1 and Ant2. The structure is connected to the metal ground through a microstrip line and Via5. The decoupling of Ant1 and Ant2 is mainly realized through the T-type parasitic element structure.

Ant3 and Ant4 adopt the form of edge-coupling feed to realize dipole current mode, and each antenna element occupies an area of 13×4.3mm². As shown in Figure 1, a 50 Ω microstrip feed line is connected to the coupled feed branch on the side plate through Via3 and Via4 at points B and C. The decoupling of the Ant3 and Ant4 is mainly realized by the ground strip between them. The strip is connected to the metal ground through Via6 on the side plate at point A.

The optimized parameters are as follows: L1=3.7mm, L2=3.7mm.

2.1. Decoupling principle between Ant1 and Ant3

Figure 2 shows the current distribution on the antenna and ground when port1 and port3 are excited at 3.5GHz, respectively. As shown in Figures 2(a) and 2(b), when the monopole (Ant1) mode is excited, the current on the antenna element is distributed in the same direction along the Z axis. While the current distribution along the X-axis is in the opposite direction, and there is a radiation zero point at the center.

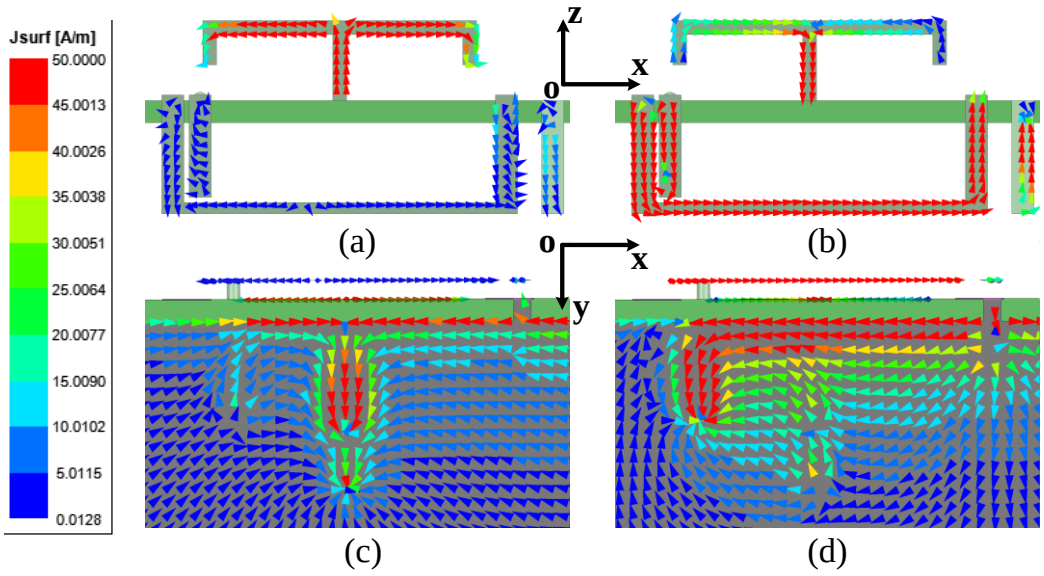


Figure 2. (a) Current distribution on the antenna when Port1 is excited at 3.5 GHz (monopole mode). (b) Current distribution on the antenna when Port3 is excited at 3.5 GHz (dipole mode). (c) Current distribution on the ground when Port1 is excited at 3.5 GHz (monopole mode). (d) Current distribution on the ground when Port3 is excited at 3.5 GHz (dipole mode).

When the dipole (Ant3) mode is excited, the current on the antenna is distributed in the same direction along the X-axis, and the radiation is the strongest at the center position. In this way, orthogonal antenna current modes are formed, so that there is no mutual coupling in space between the antennas. There is also a set of quadrature modes, which are the orthogonal currents on the ground. As shown in Figures 2(c) and 2(d), the currents on the ground are also orthogonal, so the current coupled through the ground is also blocked.

For the edge-fed dipole (Ant3), the grounded strip is the key to decoupling not only the two edge-fed dipoles Ant3 and Ant4, but also the monopole Ant1 and the edge-fed dipole Ant3. If the strip is not grounded it will affect the current balance, the isolation between the two antenna elements Ant1 and Ant3 will deteriorate rapidly. As shown in Figure 3, if the grounded point of Ant3 is removed, the isolation between Ant1 and Ant3 will rapidly deteriorate to below 10dB. It can be seen in Figure 3 that, through the introduction of Via6, the performances of S11 and S33 is somewhat worse, but these still meet the requirement of - 6dB.

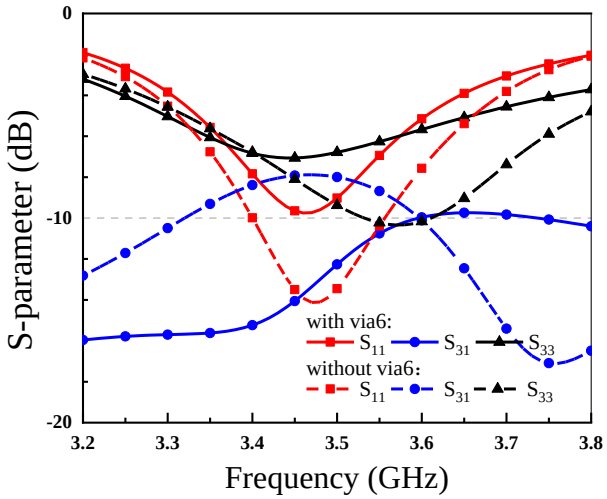


Figure 3. Simulated S-parameter of Ant1 and Ant3 with and without Via6.

2.2. Decoupling principle between Ant1 and Ant2

Figure 4 shows the current distribution on Ant1 and Ant2 with or without the grounded pin Via5 when Ant1 is excited. It can be clearly seen that when Via5 is provided, the T-type parasitic element can effectively excite the current to form a current loop with Ant1 and block the coupling current from entering Ant2.

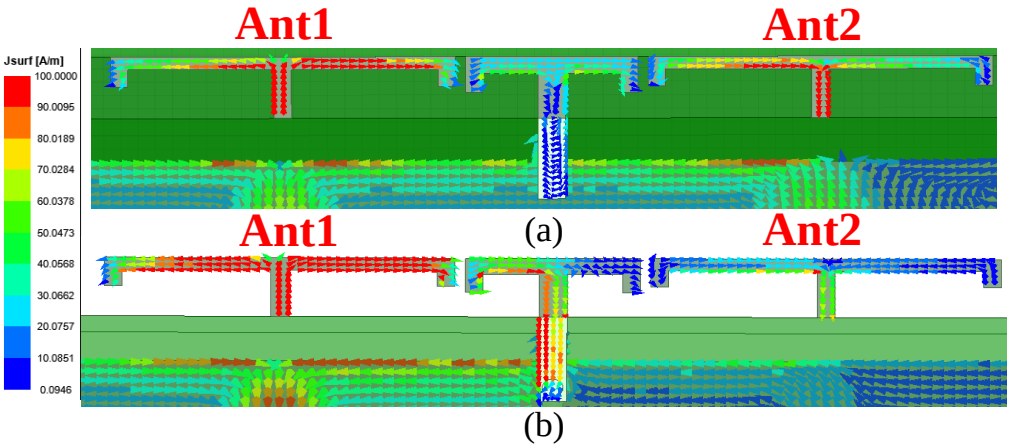


Figure 4. (a) Current distribution when Ant1 is excited without Via5. (b) Current distribution when Ant1 is excited with Via5.

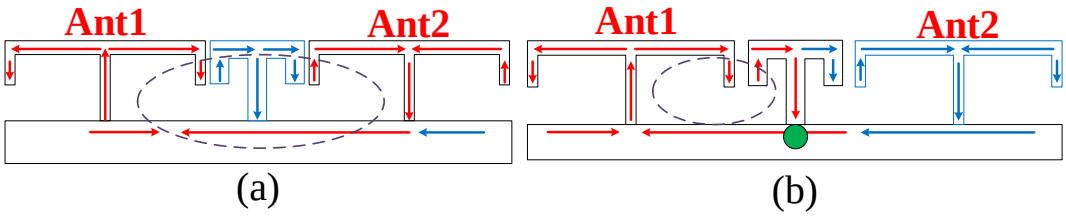


Figure 5. (a) Current model diagram when Ant1 is excited without Via5. (b) Current model diagram when Ant1 is excited with Via5.

In order to describe the decoupling mechanism more clearly, the current model diagram is established as shown in Figure 5. In Figure 4 and Figure 5, it can be seen that when there is no Via5, the space coupling current forms a current loop between the two

antenna elements, and the T-shaped decoupling branch in the middle cannot effectively excite the current. When there is a grounded pin Via5, the half side of the T-type decoupling branch close to Ant1 can effectively excite the current, forming a current loop with Ant1, and the coupling current intensity on Ant2 is significantly reduced. Figure 6 shows the simulated S-parameter of Ant1and Ant2 with or without Via5. It can be seen that when Via5 is added, the isolation between antenna elements is significantly improved. However, since the parasitic element will also have a coupling effect on the current on the excitation antenna Ant1, it will affect the impedance matching of the antenna. From the results in Figure 6, the introduction of Via5 enhances the isolation, but sacrifices part of the bandwidth of the antenna.

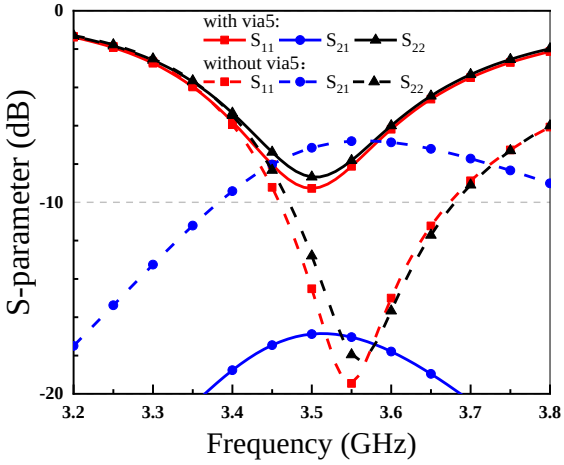


Figure 6. Simulated S-parameter of Ant1 and Ant2 with and without Via5.

2.3. Decoupling principle between Ant3 and Ant4

For the edge-fed dipoles Ant3 and Ant4, the grounded strip is the key to decoupling between Ant3 and Ant4, and its length L_1 is a key parameter. Figure 7 presents the current distribution at two resonance points 3.45GHz (resonance point 1) and 4.1GHz (resonance point 2) when Ant3 is excited. When there is no grounded strip, that is, L1=0mm, as shown in Figure 7, there are two working modes of Ant3, the resonance point of working mode 1 is 3.45GHz, and the resonance point of working mode 2 is 4.1GHz. It can be seen that working mode 1 is is not desired, because Ant3 and Ant4 are in mixed working mode at this time. The current loop of this mode is formed by the combination of the current on Ant3 and Ant4 and the current flowing through the ground plane, there must be strong coupling in this working mode. The operating mode 2 is generated by Ant3 and Ant4, separately. Ant3 and Ant4 have separate current loops in this mode, but the isolation of the antenna unit is still poor at this time, because there is a coupling current in the space.

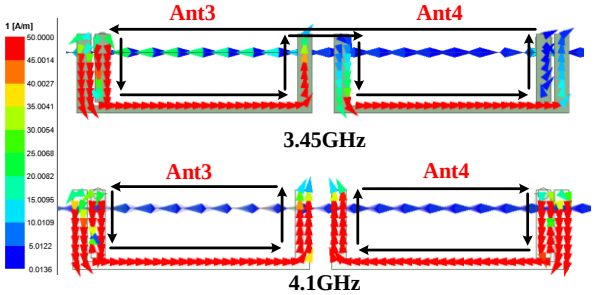


Figure 7. Simulated current distributions of Ant3 and Ant4 with port 3 excitation at 3.45 and 4.1 GHz when L1=0mm.

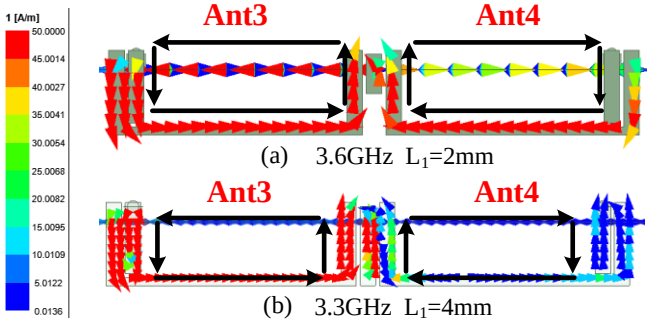


Figure 8. Simulated current distributions of Ant3 and Ant4 with port 3 excitation (a)at 3.6 GHz when L1=2mm. (b) at 3.3 GHz when L1=4mm.

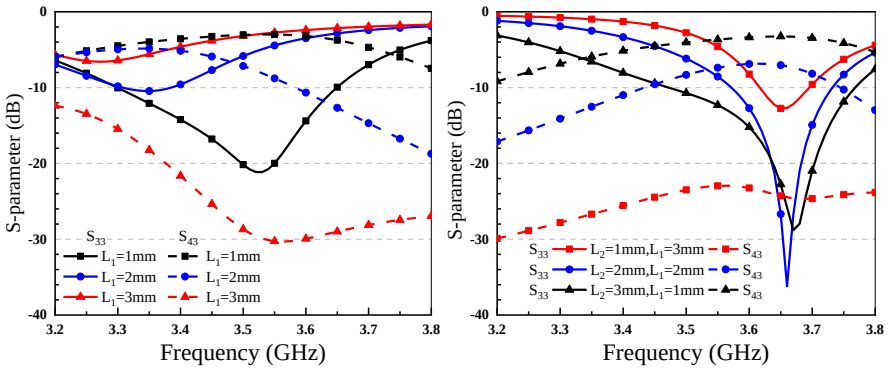


Figure 9. (a)Simulated S-parameter of Ant3 and Ant4 with different L1. (b)Simulated S-parameter of Ant3 and Ant4 with different L1 and L2.

Figure 8 shows the current distribution on the two antenna elements when Ant3 is excited. In Figure 8(a), when L_1=2mm, the resonance frequency is 3.6GHz. In Figure 8(b), when L_1=4mm, the resonance frequency 3.3GHz. At these two frequency points, the working mode 1 can no longer be effectively excited. The resonance point shifts to the low frequency band with the increase of L_1. At the same time, when L_1=4mm, only a small amount of energy is coupled into Ant4 at this time, indicating that this working mode can meet isolation requirements when the length of the ground branch is large enough.

In order to illustrate the role of the parameter L_1 more clearly, Figure 9(a) shows the simulated results of the parameter analysis of L_1. It can be seen that with the increase of L_1, the electrical size of the antenna increases, and S_{33} shifts to the low frequency band. But the S_{11} increases, sacrificing some bandwidth. And when L_1=3mm, S_{43} starts to be less than -10dB.

Since L_1 affects the matching, S_{33} and S_{43} will change with L_1 at the same time. As shown in Figure 9(b), with the complementary changes of L_1 and L_2, the resonant frequency point hardly changes. When L_1=3mm, the isolation of the entire frequency band is above 20dB. Therefore, for Ant3 and Ant4, the length of the L_1 strip must be greater than 3mm, because the isolation can meet the requirements at this time. And then adjust the length L_2 of the coupling feed branch to make the antenna work at the desired frequency band.

Table 1 shows the comparison between this work and the previous work. Comparing the antenna size and integration, the proposed antenna shows a high compactness

and realizes an excellent integration degree which integrates four elements on an area of only 28.7×7 mm².

Table 1. Comparison of the proposed antenna pair with previous works.

Ref.	Antenna Size(mm²)	Integration	Isolation	Bandwidth	ECC
[24]	20×7	Two-element integration	>17dB	3.4~3.6 GHz	<0.1
[25]	12×17	Two-element integration	>20dB	3.4~3.6 GHz	<0.06
[26]	25×7	Two-element integration	>20dB	3.4~3.6 GHz	<0.13
[27]	60×5	Four-element integration	>10dB	3.3~7.2 GHz	<0.2
[28]	38.2×3.2	Four-element integration	>11.8dB	3.4~3.6 GHz	/
This work	**28.6×7**	**Four-element integration**	>10dB	3.4~3.6 GHz	<0.35

3. Results and Discussion

In order to verify the performance of the antenna, the prototype of antenna is fabricated, as shown in Figure 10. The prototype is measured with a vector network analyzer Agilent E8363B and a microwave chamber. Figure 11 presents the measured reflection coefficient and transmission coefficient. For simplicity, the reflection coefficient and isolation of only one antenna pair are given. The results show that if -6dB is used as criteria of reflection coefficient, the bandwidth of the four antenna elements of one antenna pair can cover 3.4-3.6GHz, and the isolation between any two elements is greater than 10dB.

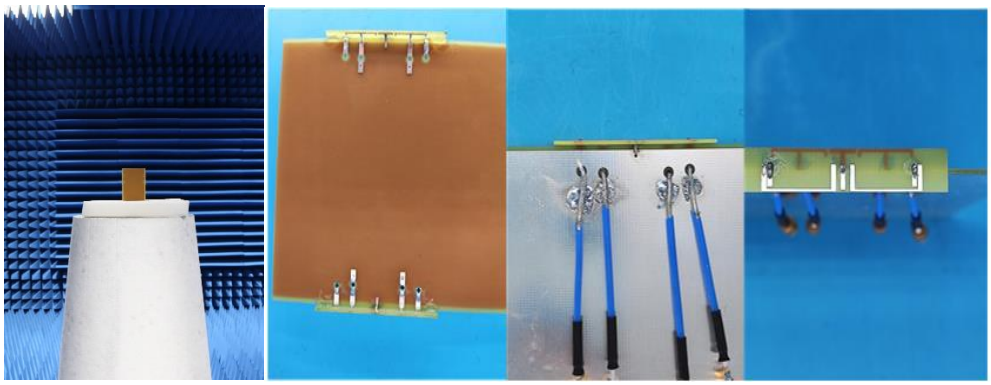


Figure 10. The fabricated prototype of the proposed antenna.

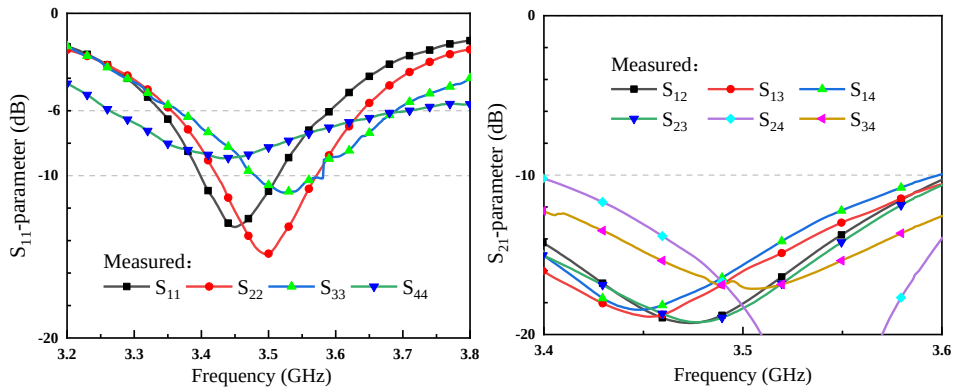


Figure 11. Measured reflection coefficient and transmission coefficient.

In order to quantitatively evaluate the diversity performance of the proposed MIMO antenna, the ECC of the antenna is calculated based on the radiated far-field using simulation software, the formula is as follows [29]:

$$E_{cc} = \rho_e = \frac{\left| \oiint \left[E_1(\theta,\varphi) \bullet E_2(\theta,\varphi) \right] d\Omega \right|^2}{\oiint |E_1(\theta,\varphi)|^2 \, d\Omega \bullet \oiint |E_2(\theta,\varphi)|^2 \, d\Omega} \quad (1)$$

where $E_i(\theta,\phi)$ is the radiation pattern of the antenna when port i is excited.

Diversity gain (DG) is an important parameter to measure good diversity characteristics and MIMO system performance. According to [30], DG can be calculated from Formula (2), and the ideal value of DG should be 10 dB.

$$DG = \sqrt{1-|\rho_e|^2} \quad (2)$$

It can be seen from Figure 12 that the ECC in the desired frequency band is less than 0.35, indicating that the presented antenna has good diversity performance. It can be seen from Figure 12 that diversity gain values are all around 10 dB, meeting the MIMO diversity criterion. Due to the symmetry of the antenna, only the antenna efficiencies of Ant1 and Ant3 are calculated. As shown in Figure 13, the efficiencies of Ant1 and Ant3 are 52.2%-57.8% and 50.2%-64.8%, respectively, over the entire operating frequency band.

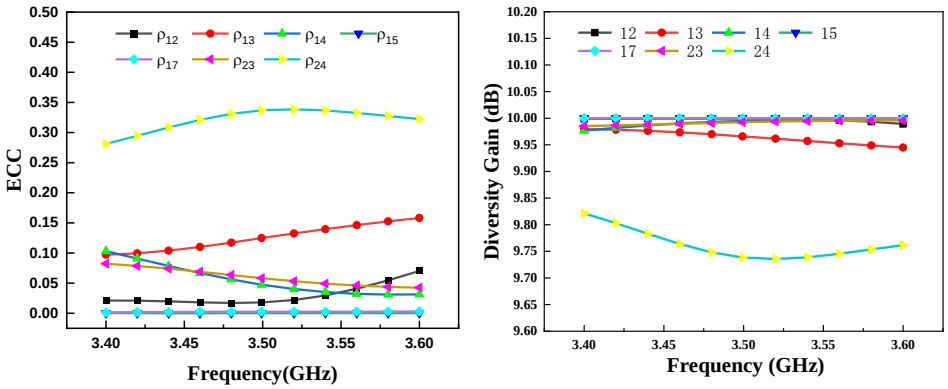


Figure 12. ECC and diversity gain of the 8×8 MIMO antenna.

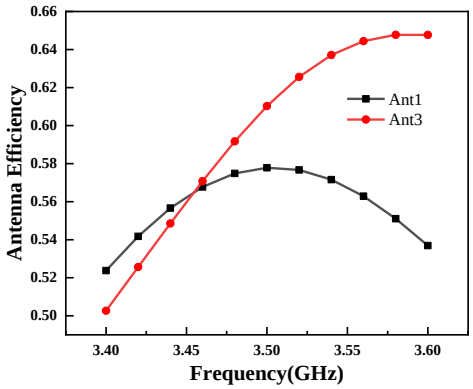


Figure 13. The efficiency of the 8×8 MIMO antenna.

Figure 14(a) shows the measured radiation pattern of Ant1 and Ant3 at 3.5 GHz in XOY plane. As shown in Figure 14(a), the radiation zero point of Ant 1 is at the center of the antenna, and the radiated energy is concentrated in the positive and negative direc-

tions of the X axis; while the Ant3 has the largest radiation energy at the center, but due to the effect of the metal floor, the energy is concentrated in the +Y direction.

Figure 14(b) shows the measured radiation pattern of Ant1 and Ant3 at 3.5 GHz in XOZ plane. As shown in Figure 14(b), the radiation zero point of Ant1 is at the center of the antenna, and the radiated energy is concentrated in the positive and negative directions of the X-axis; while the Ant3 has the largest radiation energy at the center, but due to the influence of the metal floor and surrounding radiation patches, the energy is not concentrated in the positive and negative directions of the Z axis, but is shifted. It can be known from the radiation patterns of Ant1 and Ant3 that the designed antenna has good diversity characteristics. The simulated 3D radiation patterns of Ant1 and Ant3 at 3.5 GHz are presented in Figure 15.

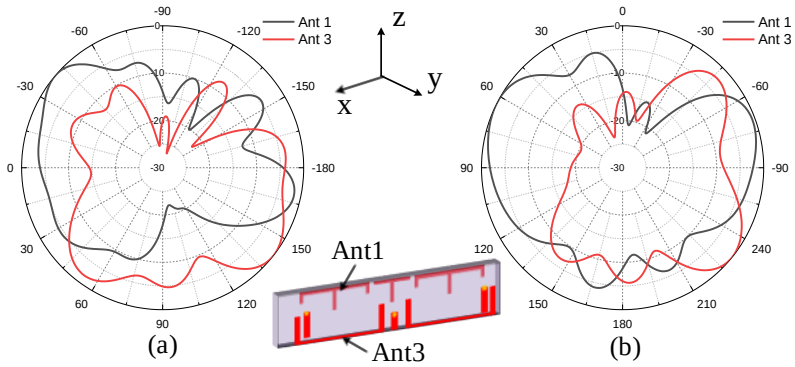
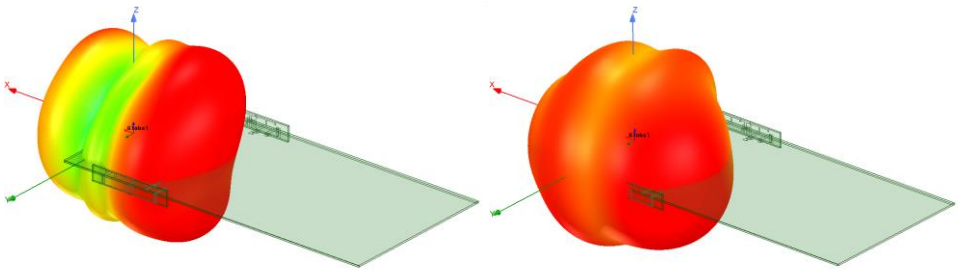


Figure 14. Measured radiation patterns of the proposed antenna at 3.5 GHz in (a) XOY plane, and (b) XOZ plane.



(a) (b)

Figure 15. Simulated **3D** radiation patterns of the proposed antenna at 3.5 GHz of (a) Ant1, and (b) Ant3.

4. Conclusions

This article presents a compact 8×8 MIMO antenna for 5G terminals which consists of a pair of quad-element antenna. The quad-element antenna is composed of two T-shaped monopoles and two edge-coupled dipoles. The quad-element is placed in a compact area. The antenna adopts polarization diversity technology, parasitic element and grounding strips to realize decoupling between antenna elements. The measured working frequency band of each element satisfies 3.4-3.6GHz, and the isolation is above 10dB. The ECC in the desired frequency band is less than 0.35 and the efficiency is over 50% in the operating bandwidth. The measured results agree well with the simulation. Owing to the convenience and flexibility of the self-decoupled design with a wideband performance, the proposed structure will be widely employed in 5G broadband MIMO

antennas. This design provides an important reference for future compact MIMO antenna design.

Author Contributions: Conceptualization, H.Z. and H.L.; methodology, H.Z., L.-X. G and H.L.; software, H.Z. and H.L.; validation, H.Z. and P.W.; formal analysis, H.Z. and P.W.; investigation, H.Z. and P.W.; resources, H.Z.; data curation, H.L.; writing—original draft preparation, H.Z. and H.L.; writing—review and editing, H.Z. and L.-X. G.; visualization, H.Z. and P.W.; supervision, L.-X. G. and H.L.; project administration, L.-X. G and P.W.; funding acquisition, L.-X. G. and P.W. All authors have read and agreed to the published version of the manuscript.

Funding: This research received no external funding.

Acknowledgments: Project supported by the National Natural Science Foundation of China (Grant No.61871457, No.U21A20457), the Foundation for Innovative Research Groups of the National Natural Science Foundation of China（Grant No.61621005）.

Data Availability Statement: Not applicable.

Conflicts of Interest: The authors declare no conflict of interest.

References

1. J. G. Andrews et al., What Will 5G Be?, IEEE Journal on Selected Areas in Communications, **2014**,Vol. 32, pp. 1065-1082.
2. M. A. Jensen and J. W. Wallace, A review of antennas and propagation for MIMO wireless communications, IEEE Transactions on Antennas and Propagation, **2004**,Vol. 52, pp. 2810-2824.
3. M. Li, L. Jiang and K. L. Yeung, A general and systematic method to design neutralization lines for isolation enhancement in MIMO antenna arrays, IEEE Transactions on Vehicular Technology, **2020**,Vol. 69, pp. 6242-6253.
4. R. Liu, X. An, H. Zheng, M. Wang, Z. Gao and E. Li, Neutralization line decoupling tri-band multiple-input multiple-output antenna design, IEEE Access, **2020**,Vol. 8, pp. 27018-27026.
5. S. Zhang and G. F. Pedersen, Mutual coupling reduction for UWB MIMO antennas with a wideband neutralization line," IEEE Antennas and Wireless Propagation Letters, **2016**,Vol. 15, pp. 166-169.
6. M. S. Khan, M. F. Shafique, A. Naqvi, A. Capobianco, B. Ijaz and B. D. Braaten, A miniaturized dual-band MIMO antenna for WLAN applications, IEEE Antennas and Wireless Propagation Letters, **2015**,Vol. 14, pp. 958-961.
7. P. Gao, S. He, X. Wei, Z. Xu, N. Wang and Y. Zheng, Compact printed UWB diversity slot antenna with 5.5-GHz band-notched characteristics," IEEE Antennas and Wireless Propagation Letters, **2014**,Vol. 13, pp. 376-379.
8. M. Li, D. Wu, B. Xiao, K. L. Yeung and L. Jiang, A novel calculation method to design parasitic decoupling technique for two antennas, IEEE Access, **2020**,Vol. 8, pp. 116041-116051.
9. K. Payandehjoo and R. Abhari, Employing EBG structures in multiantenna systems for improving isolation and diversity gain," IEEE Antennas and Wireless Propagation Letters, **2009**,Vol. 8, pp. 1162-1165.
10. Z. Yang, J. Xiao and Q. Ye, Enhancing MIMO antenna isolation characteristic by manipulating the propagation of surface wave," IEEE Access, **2020**,Vol. 8, pp. 115572-115581.
11. A. Khan, S. Bashir, S. Ghafoor and K. K. Qureshi, Mutual coupling reduction using ground stub and EBG in a compact wide-band MIMO-antenna, IEEE Access, **2021**, Vol. 9, pp. 40972-40979.
12. Y. Q. Hei, J. G. He and W. T. Li, Wideband decoupled 8-element MIMO antenna for 5G mobile terminal applications, IEEE Antennas and Wireless Propagation Letters, **2021**,Vol. 20, no. 8, pp. 1448-1452.
13. M. Y. Jamal, M. Li and K. L. Yeung, Isolation Enhancement of closely packed dual circularly polarized MIMO antenna using hybrid technique," IEEE Access, **2020**, Vol. 8, pp. 11241-11247.
14. J. Deng, J. Li, L. Zhao and L. Guo, A dual-band inverted-F MIMO antenna with enhanced isolation for WLAN applications, IEEE Antennas and Wireless Propagation Letters, **2017**,Vol. 16, pp. 2270-2273.
15. K. Wei, J. Li, L. Wang, Z. Xing and R. Xu, Mutual coupling reduction by novel fractal defected ground structure bandgap filter, IEEE Transactions on Antennas and Propagation, **2016**,Vol. 64, no. 10, pp. 4328-4335.
16. Y. Cheng and K. M. Cheng, Compact Wideband decoupling and matching network design for dual-antenna array, IEEE Antennas and Wireless Propagation Letters, **2020**,Vol. 19, no. 5, pp. 791-795.
17. Y. Zhang, S. Zhang, J. Li and G. F. Pedersen, A transmission-line-based decoupling method for MIMO antenna arrays, IEEE Transactions on Antennas and Propagation, **2019**,Vol. 67, no. 5, pp. 3117-3131.
18. M. Li, J. M. Yasir, K. L. Yeung and L. Jiang, A novel dual-band decoupling technique, IEEE Transactions on Antennas and Propagation, **2020**,Vol. 68, no. 10, pp. 6923-6934.
19. M. Koohestani, A. A. Moreira and A. K. Skrivervik, A novel compact CPW-fed polarization diversity ultrawideband antenna, IEEE Antennas and Wireless Propagation Letters, **2014**,Vol. 13, pp. 563-566.
20. L. Liu, S. W. Cheung and T. I. Yuk, Compact MIMO antenna for portable devices in UWB applications, IEEE Transactions on Antennas and Propagation, **2013**,Vol. 61, pp. 4257-4264.
21. J. Zhu, S. Li, B. Feng, L. Deng and S. Yin, Compact dual-polarized UWB quasi-self-complementary MIMO diversity antenna with band-rejection capability," IEEE Antennas and Wireless Propagation Letters, **2016**,Vol. 15, pp. 905-908, 2016.
22. Y. Yao, X. Wang, X. Chen, J. Yu and S. Liu, Novel diversity MIMO PIFA antenna with broadband circular polarization for multimode satellite navigation," IEEE Antennas and Wireless Propagation Letters, **2012**,Vol. 11, pp. 65-68.
23. https://www.ansys.com/
24. Z. Ren, A. Zhao and S. Wu, MIMO antenna with compact decoupled antenna pairs for 5G mobile terminals," IEEE Antennas and Wireless Propagation Letters, **2019**, Vol. 18, no. 7, pp. 1367-1371.
25. L. Sun, H. Feng, Y. Li and Z. Zhang, Compact 5G MIMO mobile phone antennas with tightly arranged orthogonal-mode pairs," IEEE Transactions on Antennas and Propagation, **2018**,Vol. 66, pp. 6364-6369.
26. L. Chang, Y. Yu, K. Wei and H. Wang, Polarization-orthogonal co-frequency dual antenna pair suitable for 5G MIMO smartphone with metallic bezels, IEEE Transactions on Antennas and Propagation, **2019**,Vol. 67, pp. 5212-5220.
27. L. Sun, Y. Li and Z. Zhang, Wideband integrated quad-element MIMO antennas based on complementary antenna pairs for 5G smartphones, IEEE Transactions on Antennas and Propagation, **2021**, Vol. 69, pp. 4466-4474.
28. C. Deng, D. Liu and X. Lv, Tightly arranged four-element MIMO antennas for 5G mobile terminals, IEEE Transactions on Antennas and Propagation, **2019**,Vol. 67, pp. 6353-6361.
29. L. Sun, Y. Li, Z. Zhang and H. Wang, Antenna decoupling by common and differential modes cancellation, IEEE Transactions on Antennas and Propagation, 2021, Vol. 69, pp. 672-682.

30. M. Ameen, O. Ahmad, and RK. Chaudhary, Bandwidth and gain enhancement of triple-band MIMO antenna incorporating metasurface-based reflector for WLAN/WiMAX applications, 2020, IET Microwave Antennas Propagation,Vol,14, pp.1493-1503.